Electronic Research Archive

https://www.aimspress.com/journal/era

ERA, 32(7): 4365–4377.
DOI: 10.3934/era.2024196
Received: 23 April 2024
Revised: 24 June 2024
Accepted: 28 June 2024
Published: 11 July 2024

Research article

A regularized eigenmatrix method for unstructured sparse recovery

Koung Hee Leem, Jun Liu* and George Pelekanos

Department of Mathematics and Statistics, Southern Illinois University Edwardsville, Edwardsville, IL 62026, USA

* **Correspondence:** Email: juliu@siue.edu.

Abstract: The recently developed data-driven eigenmatrix method shows very promising reconstruction accuracy in sparse recovery for a wide range of kernel functions and random sample locations. However, its current implementation can lead to numerical instability if the threshold tolerance is not appropriately chosen. To incorporate regularization techniques, we have proposed to regularize the eigenmatrix method by replacing the computation of an ill-conditioned pseudo-inverse by the solution of an ill-conditioned least squares system, which can be efficiently treated by Tikhonov regularization. Extensive numerical examples confirmed the improved effectiveness of our proposed method, especially when the noise levels were relatively high.

Keywords: eigenmatrix method; Tikhonov regularization; L-curve rule; ESPRIT algorithm

1. Background

Let X be the parameter space and S be the sampling space. Assume $g(s, x)$ is a given kernel function on $S \times X$ that is analytic in x. Suppose the unknown sparse signal f is given by

$$f(x) = \sum_{k=1}^{n_x} w_k \delta(x - x_k), \tag{1.1}$$

with δ being the Dirac delta function, and n_x spikes with distinct locations $\{x_k\}$ and weights $\{w_k\}$. The observable for any given sampling point $s \in S$ is given by the following summation

$$u(s) := \int_X g(s, x) f(x)\, dx = \sum_{k=1}^{n_x} w_k g(s, x_k). \tag{1.2}$$

Let $\{s_j\}$ be a chosen set of n_s (unstructured) sample locations in S and $u_j = u(s_j)$ be the unknown exact values of observations. In practice, we can only obtain noisy observations, which are assumed to have the following multiplicative form (with an unknown noise magnitude $\sigma > 0$):

$$\widetilde{u}_j = u_j(1 + \sigma \mathcal{Z}_j), \tag{1.3}$$

with $\mathcal{Z}_j$ being independently identically distributed (i.i.d.) standard Gaussian random variables with zero mean and unit variance. Notice in (1.3) the relative noise $(\widetilde{u}_j - u_j)/u_j = \sigma\mathcal{Z}_j$ is assumed to be normally distributed with a standard deviation σ. Our task is to recover the unknown spike locations $\boldsymbol{x} := [x_1; x_2; \cdots; x_{n_x}]$ and weights $\boldsymbol{w} := [w_1; w_2; \cdots; w_{n_x}]$ from the observation $\{\widetilde{u}_j\}$. Obviously, this leads to a highly nonlinear inverse problem that is difficult to treat numerically. The standard nonlinear least square formulation will lead to a nonconvex unconstrained optimization problem that can be better solved with a good initial guess estimated by the studied eigenmatrix methods.

Depending on the definition of kernel function g, the sparse recovery problem in the above general form (1.2) covers a list of well-known sparse recovery problems, such as rational approximation [1], spectral function estimation [2, 3], Fourier inversion [4, 5], Laplace inversion [6–9], and sparse deconvolution, for which many specially designed numerical algorithms [10, 11] were established with good theoretical support in the past few decades; see references in [12]. Nevertheless, these tailored algorithms rely heavily on the underlying structure of each problem, which are not directly applicable to general kernel functions with an unstructured sampling grid. The developed data-driven eigenmatrix method in [12] does not assume any structures in the kernel function and sampling grid and hence it has a wider applicability that specialized or structured sparse recovery algorithms. Nevertheless, it requires the computation of the psedudo-inverse of a highly ill-conditioned rectangle matrix, which can lead to numerical instability when the threshold tolerance does not match with the underlying noise levels in the measurement data. Our major contribution is to propose a regularized eigenmatrix method that can handle noisy measurement data through modern Tikhonov regularization techniques, which demonstrates significantly improved recovery accuracy in tested numerical examples with high noise levels.

This paper is organized as follows. In Section 2, we briefly review the original eigenmatrix method and point out its drawbacks. In Section 3, we introduce a new regularized eigenmatrix method based on Tikhonov regularization techniques. A few numerical examples are presented in Section 4. Finally, some remarks are concluded in Section 5.

2. Review of the eigenmatrix method

Inspired by the shifting operator defined in Prony's method and the ESPRIT algorithm [13], the recently developed eigenmatrix method [12] for unstructured sparse recovery problems shows very appealing reconstruction accuracy for different kernels and unstructured sampling locations. Its key idea is to find an n_s-by-n_s eigenmatrix M such that for all $x \in X$ there approximately holds the *eigensystem*

$$M\boldsymbol{g}(x) \approx x\boldsymbol{g}(x), \tag{2.1}$$

where $\boldsymbol{g}(x) = [g(s_j, x)]_{1\le j\le n_s}$ is an n_s-by-1 vector of functions on X. In numerical implementations, we can enforce this approximate relation over a set of collocation nodes $\{a_t\}_{t=1}^{n_a}$ selected in X. More specifically, if X is the unit disk $\mathbb{D}$ on a complex plane, one can select a uniform grid of collocation nodes on the boundary of the unit disk, which can be justified by invoking the exponentially convergent trapezoidal rule and the application of the Cauchy integral theorem for analytic functions. If X is the real interval $[-1, 1]$, one can choose a Chebyshev grid of collocation nodes on $[-1, 1]$, which can be explained by the Chebyshev quadrature for analytic functions. A general connected domain X can be treated by introducing a smooth one-to-one map between X and $\mathbb{D}$ or $[-1, 1]$. At this point, there are no error estimates on the accuracy of the approximation (2.1) in various settings.

Following the notation and methodology introduced in [12], the original eigenmatrix method based on the ESPRIT method mainly consists of the following 4 major steps (not including the post-processing step for simplicity):

The original eigenmatrix method

1) Compute the matrix $G = [g(s_j, a_t)] \in \mathbb{C}^{n_s \times n_a}$ based on the n_s sampling locations $\{s_j\}_{j=1}^{n_s}$ and n_a collocation nodes $\{a_t\}_{t=1}^{n_a}$. Normalize G column-wisely to get $\widehat{G}$.
2) Compute the $n_s \times n_s$ eigenmatrix $M = \widehat{G}\Lambda\widehat{G}^{\dagger}$, where $\Lambda = \mathrm{diag}(a_t)$ and $\widehat{G}^{\dagger}$ is the pseudo-inverse of $\widehat{G}$ by thresholding singular values smaller than a given tolerance *tol*.
3) Given the vector of noisy observations $\widetilde{\boldsymbol{u}}$, choose $l > n_x$ and then compute rank-n_x truncated SVD of the following matrix

$$A := \left[\begin{array}{cccc} \widetilde{\boldsymbol{u}}, & M\widetilde{\boldsymbol{u}}, & \cdots, & M^l\widetilde{\boldsymbol{u}} \end{array} \right] = USV^*. \tag{2.2}$$

   Define V_+^* and V_-^* to be the sub-matrix of V^* by deleting the first column and the last column, respectively. The n_x eigenvalues $\{\widetilde{x}_k\}$ of the matrix $V_+^*(V_-^*)^{\dagger}$ yield the estimated spike locations. Here, we expect (V_-^*) to be well-conditioned.
4) With computed $\{\widetilde{x}_k\}$, the weights $\widetilde{\boldsymbol{w}} = [\widetilde{w}_1; \widetilde{w}_2; \cdots; \widetilde{w}_{n_x}]$ can be estimated via a least squares problem defined by $\widetilde{G}\widetilde{\boldsymbol{w}} = \widetilde{\boldsymbol{u}}$, where $\widetilde{G} = [g(s_j, \widetilde{x}_k)]$ is of size $n_s \times n_x$.

As a data-driven approach, it involves the key procedure of (approximately) finding the pseudo-inverse $\widehat{G}^{\dagger}$ of a highly ill-conditioned rectangular matrix $\widehat{G}$, which was not carefully treated from the perspective of regularization. To alleviate the issue of large condition numbers of $\widehat{G}$, in [12] the author suggested to choose (a small) $n_a = 32$ such that $\widehat{G}$ is of full column rank and its condition number is bounded below by 10^7. Moreover, the thresholding tolerance *tol* was selected such that $\|M\|$ is bounded by a small constant such as 3. In their MATLAB implementations*, the authors used the built-in pseudoinverse function pinv based on truncated singular value decomposition (TSVD) with $tol = 10^{-4}\|\widehat{G}\|_F$ or $tol = 10^{-8}\|\widehat{G}\|_F$ as the thresholding tolerance in different examples. Based on the discussion in [12], the tolerance *tol* for each example is chosen to be slightly smaller or comparable to the noise level, such that the reconstruction is relatively well-conditioned and the computed eigenmatrix does not cause significantly larger error than the measurement noise. Hence, the current strategy, of selecting a small n_a and a small *tol*, essentially points to some heuristic regularization treatment that requires manual tuning, which may be less robust in handling a wide range of unknown noise levels. Nevertheless, the design of the regularization scheme is not the main focus of [12], which for the first time presents the novel eigenmatrix method for sparse signal recovery. Our following proposed regularized eigenmatrix method provides a more systematic and robust regularization strategy that avoids the direct computation of the pseudo-inverse $\widehat{G}^{\dagger}$.

As suggested in [12], when the number of spikes n_x is not known a priori, a general rule is to select n_x as small as possible such that the total least squares fitting error (after post-processing) falls within the noise level. The commonly used criteria include Akaike information criterion (AIC) [14] and Bayesian information criterion (BIC) [15, 16]. We will assume n_x is already fixed.

*https://github.com/lexingying/EigenMatrix

3. A regularized eigenmatrix method

To make use of modern regularization techniques in the above eigenmatrix method, we need to avoid explicitly computing the ill-conditioned pseudo-inverse matrix $\widehat{G}^{\dagger}$. In view of the matrix A in (2.2), we only need the matrix-vector products $M^k\widetilde{\boldsymbol{u}}$ for $k \geq 1$, which implies that the explicit construction of matrix M is unnecessary. By the theory of pseudo-inverses, if $\widehat{G}$ has **linearly independent columns**, then there holds $\widehat{G}^{\dagger}\widehat{G} = I_{n_a}$, which leads to

$$M^k\widetilde{\boldsymbol{u}} = (\widehat{G}\Lambda\widehat{G}^{\dagger})^k\widetilde{\boldsymbol{u}} = \underbrace{\widehat{G}\Lambda\widehat{G}^{\dagger}\widehat{G}\Lambda\widehat{G}^{\dagger}\cdots\widehat{G}\Lambda\widehat{G}^{\dagger}}_{k \text{ times}}\widetilde{\boldsymbol{u}} = \widehat{G}\Lambda^k\widehat{G}^{\dagger}\widetilde{\boldsymbol{u}}.$$

Let $\boldsymbol{v} = \widehat{G}^{\dagger}\widetilde{\boldsymbol{u}}$, then we can rewrite matrix A in (2.2) in the form

$$A = \left[\ \widetilde{\boldsymbol{u}},\ \ \widehat{G}\Lambda\boldsymbol{v},\ \ \cdots,\ \ \widehat{G}\Lambda^l\boldsymbol{v}\ \right]. \tag{3.1}$$

The vector $\boldsymbol{v} = \widehat{G}^{\dagger}\widetilde{\boldsymbol{u}}$ can then be obtained from the following ill-conditioned linear system

$$\widehat{G}\boldsymbol{v} = \widetilde{\boldsymbol{u}}, \tag{3.2}$$

since then we can obtain $\boldsymbol{v} = I_{n_a}\boldsymbol{v} = \widehat{G}^{\dagger}(\widehat{G}\boldsymbol{v}) = \widehat{G}^{\dagger}\widetilde{\boldsymbol{u}}$. From above, it follows that there is not even a need to approximately compute the pseudo-inverse $\widehat{G}^{\dagger}$ or construct the matrix M.

In summary, we propose the following regularized eigenmatrix method without M, which should be compared with the original eigenmatrix method [12] as listed in Section 2:

Our proposed regularized eigenmatrix method

1) Unchanged.
2) Solve system (3.2) for $\boldsymbol{v}$ by the Tikhonov regularization method (see below).
3) Construct A using (3.1), and leave the remaining parts unchanged.
4) Unchanged.

We reiterate here, that the significant improvement from the original eigenmatrix method is to avoid explicitly computing the eigenmatrix M that requires the computation of the pseudo-inverse $\widehat{G}^{\dagger}$. Moreover, the noisy observation $\widetilde{\boldsymbol{u}}$ will influence the computation of $\boldsymbol{v}$ through the employed Tikhonov regularization techniques, which take into consideration the (unknown) noise level in $\widetilde{\boldsymbol{u}}$ automatically through the used regularization parameter choice rules. Numerically, we found our proposed method still works well even when $\widehat{G}$ has linearly dependent columns.

To demonstrate the role of vector $\boldsymbol{v}$ in the above method, we consider $\widetilde{\boldsymbol{u}} = \widehat{G}\boldsymbol{v}$, and we let $\boldsymbol{a}^k = \text{diag}(\Lambda^k) := [a_1^k; a_2^k; \cdots; a_{n_a}^k]$ be a column vector. We then obtain the following factorization

$$A = \widehat{G}\left[\ \boldsymbol{v},\ \ \Lambda\boldsymbol{v},\ \ \cdots,\ \ \Lambda^l\boldsymbol{v}\ \right] = \widehat{G}\,\text{diag}(\boldsymbol{v})\,[\mathbf{1}, \boldsymbol{a}, \cdots, \boldsymbol{a}^l], \tag{3.3}$$

which closely fits the desired factorization structure of the eigenmatrix method [12], that is

$$A \approx \widetilde{G}\,\text{diag}(\widetilde{\boldsymbol{w}})\,[\mathbf{1}, \boldsymbol{x}, \cdots, \boldsymbol{x}^l]. \tag{3.4}$$

Hence, the entries of the vector $\boldsymbol{v}$ act as the "weights" for the corresponding collocation nodes $\{a_t\}$. This connection may be helpful to choose better sampling points $\{s_j\}$ and collocation nodes $\{a_t\}$. For instance, if $n_a = n_x$ such that the chosen collocation nodes are identical to the unknown spike locations, we would expect to obtain very accurate reconstruction.

3.1. Tikhonov regularization for solving (3.2)

We are now ready to employ modern regularization techniques [17–21] to solve (3.2). The standard Tikhonov regularization method approximates the solution $\boldsymbol{v}$ of (3.2) by the unique minimizer of the following Tikhonov regularized objective functional

$$\min_{\boldsymbol{v}} \left\{ \|\widehat{G}\boldsymbol{v} - \widetilde{\boldsymbol{u}}\|^2 + \gamma \|\boldsymbol{v}\|^2 \right\}, \tag{3.5}$$

where $\gamma > 0$ is a regularization parameter to be determined. Due to the strong convexity with $\gamma > 0$, the unique solution $\boldsymbol{v}_\gamma$ of (3.5) is given by the following regularized normal equation

$$(\widehat{G}^*\widehat{G} + \gamma I)\boldsymbol{v}_\gamma = \widehat{G}^*\widetilde{\boldsymbol{u}}. \tag{3.6}$$

There are many different a priori or a posteriori methods of choosing a good regularization parameter $\gamma > 0$, such as Morozov's discrepancy principle [22] that requires the knowledge of noise level. In our numerical experiments, we will only apply and compare the established improved maximum product criterion (IMPC) [23] and L-curve [24, 25] techniques[†] for estimating the regularization parameter γ, since both methods do not require a priori knowledge of the (unknown) noise level in the measured data $\widetilde{\boldsymbol{u}}$. Both methods yield regularization parameters that are very close to each other, and hence deliver similar reconstruction accuracy. For large-scale problems, computationally more efficient iterative regularization techniques [26, 27] (with early stopping) may also be used.

Our major contribution is not to develop a new regularization method, but to reformulate the original eigenmatrix method such that the modern regularization techniques can be seamlessly employed. Such modern regularization techniques include the asymptotical regularization methods [28, 29], accelerated regularization methods [30, 31], stochastic regularization methods [32–36], and so on. Finally, we remark that the author in [18] presented extensive discussion on the comparison between the Tikhonov regularization method and the pseudoinverse-type regularization method (i.e., to approximately compute the matrix-vector product $\widehat{G}^\dagger\widetilde{\boldsymbol{u}}$ via TSVD). In [37], the authors suggested that the Tikhonov regularization works better than pseudoinversion when the condition number is larger than a critical value. For our studied problems, the condition numbers are very large (ranging from 10^7 to 10^{17}) and hence we expect the Tikhonov regularization method to perform better in general.

4. Numerical results

In this section, we will numerically compare the original eigenmatrix method based on pseudoinverse (denoted by pinv) and our proposed regularized eigenmatrix method based on IMPC and L-curve techniques. All simulations are implemented using MATLAB R2024a. To better illustrate the influence of our proposed regularization techniques on the reconstruction accuracy, we will only compare the recovered spike locations and weights based on the ESPRIT algorithm, without the extra post-processing step of nonlinear optimization that may further improve the reconstruction accuracy. To measure the reconstruction accuracy, we report the absolute difference of the spike locations and weights separately in Euclidean norm as the overall reconstruction errors, that is

$$\text{errors} = (\|\boldsymbol{x} - \widetilde{\boldsymbol{x}}\|_2, \|\boldsymbol{w} - \widetilde{\boldsymbol{w}}\|_2).$$

[†] http://www2.compute.dtu.dk/~pcha/Regutools/

We would expect the obtained errors to get smaller as the noise level δ is decreased. We will test the same examples and sampling locations as described in [12], except that the used noise levels are increased by 10 times to better demonstrate the robustness of our proposed regularization techniques. In particular, the spike weights $\{w_k\}$ are set to be one and the noisy observation $\widetilde{u}_j$ is constructed by adding different levels of Gaussian noise to the exact observation $u_j = u(s_j)$. The obtained errors are affected by both the used algorithms and the measurement noise, which may show some variance in numerical simulations. To minimize the influence of randomness, we compare all of the algorithms with the same random noise for a given noise level δ. For better visual comparison, we used MATLAB's `linkaxes` function to unify the limits of axes in all of the subplots.

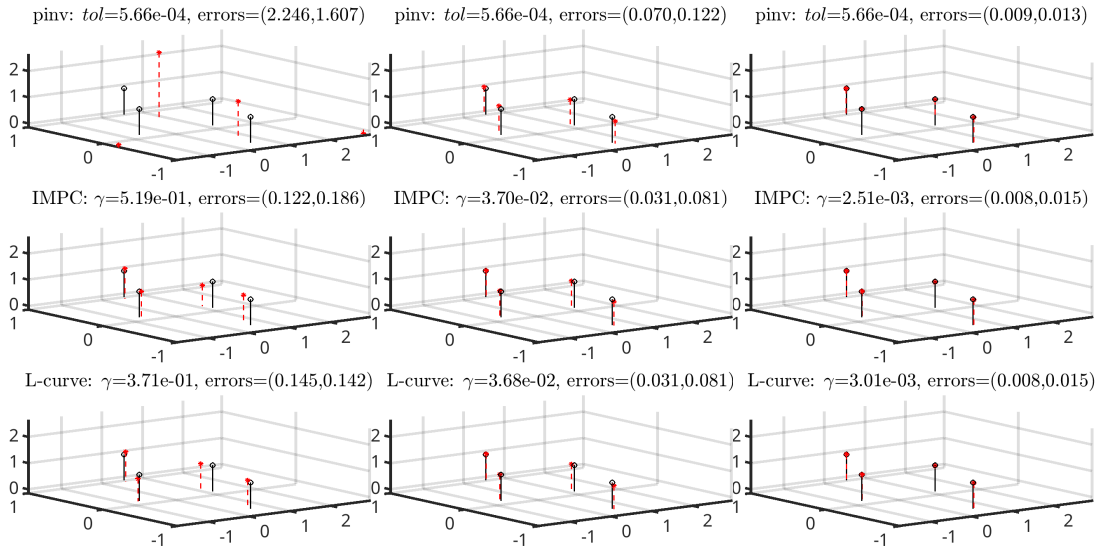

Figure 1. Rational approximation (columns from left to right: $\sigma = 10^{-1}, 10^{-2}, 10^{-3}$). The exact spikes are in a solid line and the recovered spikes are in a dashed line. The errors measure the 2-norm difference in spike locations and weights, respectively.

4.1. Example 1 (Rational approximation)

In this problem, we have $X = \mathbb{D}$, $g(s, x) = \frac{1}{s-x}$, and true spike locations

$$\boldsymbol{x} = 0.9e^{2\pi i[0.2;0.5;0.8;1]}.$$

We generated $n_s = 40$ random sampling points $\{s_j\}$ outside the unit disk, each with a modulus between 1.2 and 2.2. We then built the matrix $G = [g(s_j, a_t)]$ with $n_a = 32$ uniformly spaced collocation nodes on the unit circle. Numerically, we notice that $\widehat{G}$ is of full column rank with $\text{rank}(\widehat{G}) = 32$ and a moderate condition number $\text{cond}(\widehat{G}) \approx 10^7$. Figure 1 shows the reconstructed spike locations and weights in comparison with the exact ones by 3 different methods (from top to bottom: pinv, IMPC, and L-curve) with 3 different noise levels (from left to right). Clearly, our regularized eigenmatrix methods (both IMPC and L-curve) deliver improved recovery (with smaller errors in each column), especially when the noise level gets higher. Both the IMPC and L-curve techniques yield comparable

regularization parameter γ. Notice the threshold tolerance $tol = 10^{-4}\|\widehat{G}\|_F$ used in the original eigenmatrix method is independent of the noise level, which may cause degraded reconstruction accuracy if not appropriately chosen. We also report in Table 1 the reconstruction errors with a range of n_s and n_a based on the L-curve method, which shows the errors (in the last row) gradually decrease to the noise level when both n_s and n_a are sufficiently large. Here, the different rows involve different random noise of the same noise level δ. In particular, the errors in each row are largely saturated when $n_a > 30$, and a much larger n_a does not seem to worsen the reconstruction, which indicates the eigenmatrix method is insensitive to the choice of a sufficiently large n_a.

Table 1. Reconstruction errors with different n_s and n_a by the L-curve method ($\delta = 10^{-3}$).

$n_s \backslash n_a$	10	20	30	40	50	60
20	(0.859, 2.327)	(0.045, 0.129)	(0.039, 0.110)	(0.039, 0.110)	(0.038, 0.109)	(0.038, 0.109)
40	(0.548, 2.937)	(0.008, 0.019)	(0.008, 0.014)	(0.008, 0.014)	(0.008, 0.014)	(0.008, 0.014)
60	(0.603, 1.662)	(0.007, 0.017)	(0.007, 0.018)	(0.007, 0.018)	(0.007, 0.018)	(0.007, 0.018)
80	(0.984, 1.981)	(0.005, 0.003)	(0.002, 0.003)	(0.002, 0.002)	(0.002, 0.002)	(0.002, 0.002)
100	(0.785, 2.954)	(0.004, 0.004)	(0.003, 0.008)	(0.003, 0.008)	(0.003, 0.008)	(0.003, 0.008)
120	(0.987, 2.869)	(0.005, 0.008)	(0.001, 0.002)	(0.001, 0.002)	(0.001, 0.002)	(0.001, 0.002)
140	(0.851, 4.654)	(0.004, 0.009)	(0.002, 0.003)	(0.002, 0.004)	(0.002, 0.004)	(0.002, 0.003)
160	(0.699, 2.871)	(0.007, 0.017)	(0.002, 0.002)	(0.001, 0.002)	(0.001, 0.002)	(0.001, 0.002)
180	(0.787, 2.698)	(0.005, 0.009)	(0.001, 0.003)	(0.001, 0.003)	(0.001, 0.003)	(0.001, 0.003)
200	(0.970, 3.415)	(0.005, 0.005)	(0.001, 0.001)	(0.001, 0.001)	(0.001, 0.001)	(0.001, 0.001)

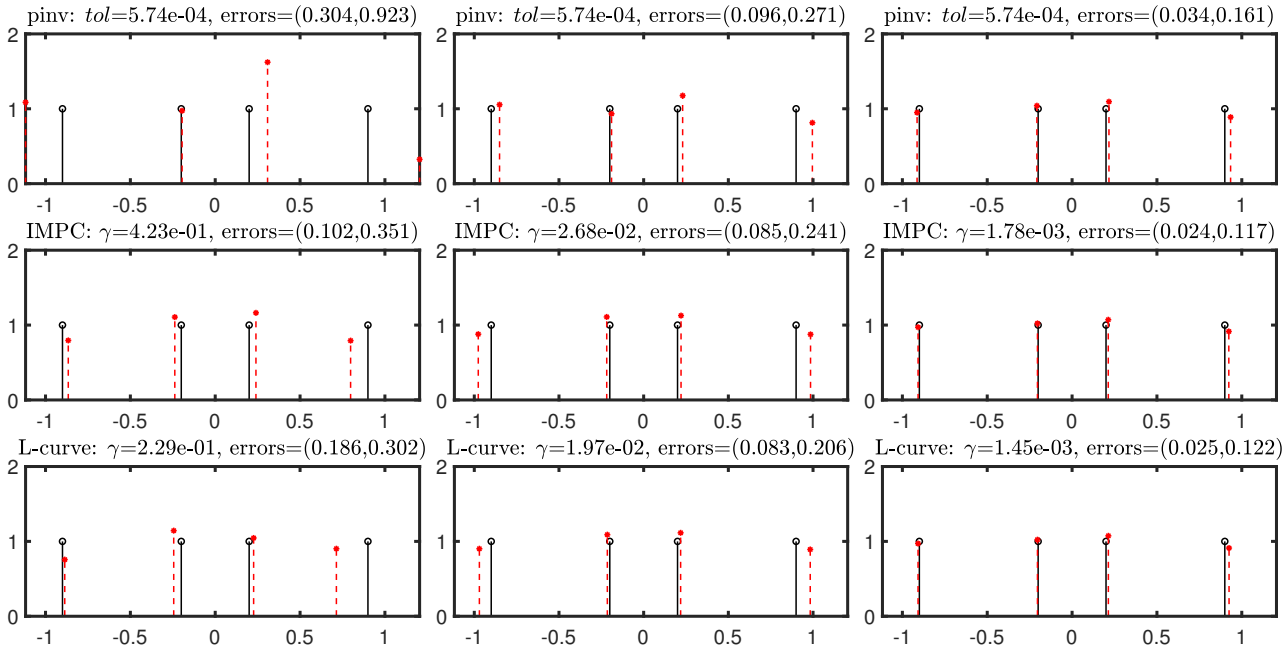

Figure 2. Spectral function approximation (columns from left to right: $\sigma = 10^{-1}, 10^{-2}, 10^{-3}$). The exact spikes are in a solid line and the recovered spikes are in a dashed line. The errors measure the 2-norm difference in spike locations and weights, respectively.

4.2. Example 2 (Spectral function approximation)

In this problem, we have $X = [-1, 1]$, $g(s, x) = \frac{1}{s-x}$, and true spike locations

$$\boldsymbol{x} = [-0.9; -0.2; 0.2; 0.9].$$

We use $n_s = 256$ uniformly distributed sampling points $s_j = \pm(2j-1)\pi i/\beta$, $j = 1, 2, \cdots, 128$ from the Matsubara grid on the imaginary axis, and then build the matrix $G = [g(s_j, a_t)]$ with $n_a = 32$ Chebyshev collocation nodes on $[-1, 1]$. Numerically, we notice that $\widehat{G}$ is not of full column rank with $\text{rank}(\widehat{G}) = 31$ and a large condition number $\text{cond}(\widehat{G}) \approx 10^{15}$. Figure 2 shows the reconstructed spike locations and weights in comparison with the exact ones by 3 different methods (denoted by pinv, IMPC, and L-curve) with 3 different noise levels. Clearly, our regularized eigenmatrix methods (both IMPC and L-curve) provide more accurate recovery, especially when the noise levels are high.

4.3. Example 3 (Fourier inversion)

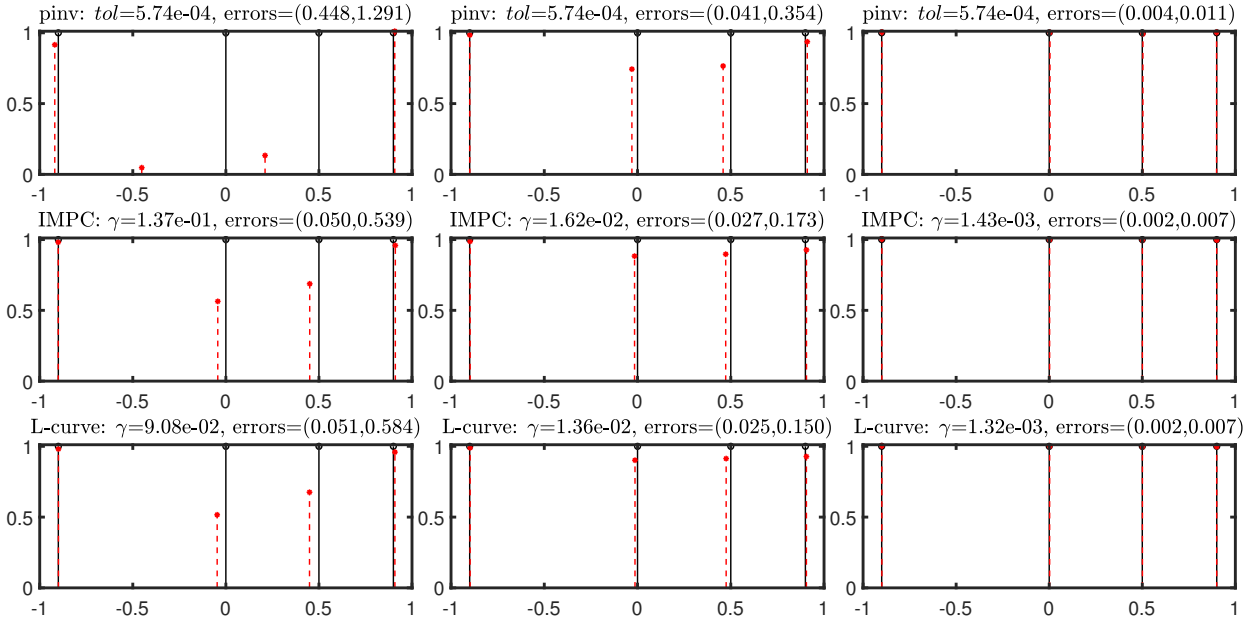

Figure 3. Fourier inversion (columns from left to right: $\sigma = 10^{-1}, 10^{-2}, 10^{-3}$). The exact spikes are in a solid line and the recovered spikes are in a dashed line. The errors measure the 2-norm difference in spike locations and weights, respectively.

In this problem, we have $X = [-1, 1]$, $g(s, x) = e^{i\pi sx}$, and true spike locations

$$\boldsymbol{x} = [-0.9; 0; 0.5; 0.9].$$

We generated $n_s = 128$ random sampling points $\{s_j\}$ in $[-5, 5]$, and then build the matrix $G = [g(s_j, a_t)]$ with $n_a = 32$ Chebyshev collocation nodes on $[-1, 1]$. Numerically, we notice that $\widehat{G}$ is of full column rank with $\text{rank}(\widehat{G}) = 32$ and a moderate condition number $\text{cond}(\widehat{G}) \approx 10^7$. Figure 3 presents the reconstructed spike locations and weights in comparison with the exact ones by 3 different methods

(denoted by pinv, IMPC, and L-curve) with 3 different noise levels. Again, our regularized eigenmatrix method (both IMPC and L-curve) delivers more accurate recovery. It is worthwhile to point out that the original eigenmatrix method also works very well for this problem with small noise levels, likely due to the relatively smaller condition number cond($\widehat{G}$) $\approx 10^7$.

4.4. Example 4 (Laplace inversion)

In this problem, we have $X = [0.1, 2.1]$, $g(s, x) = xe^{-sx}$, and true spike locations

$$\boldsymbol{x} = [0.2; 1.1; 1.6; 2.0].$$

We generated $n_s = 100$ random sampling points $\{s_j\}$ in $[0, 10]$ and then build the matrix $G = [g(s_j, a_t)]$ with $n_a = 32$ shifted Chebyshev collocation nodes on $[0.1, 2.1]$. Notice here that $\widehat{G}$ is not of full column rank with rank($\widehat{G}$) = 17 and a large condition number cond($\widehat{G}$) $\approx 10^{17}$. In [12], the author only tested very low noise levels ($\sigma = 10^{-5}, 10^{-6}, 10^{-7}$) with a very small threshold tolerance $tol = 10^{-8}\|\widehat{G}\|_F$, which may conceal the essential difficulty of highly ill-conditioned G. Hence, we will test with higher noise levels ($\sigma = 10^{-3}, 10^{-4}, 10^{-5}$), where we found the moderate threshold tolerance $tol = 10^{-4}\|\widehat{G}\|_F$ works better in treating higher noise levels.

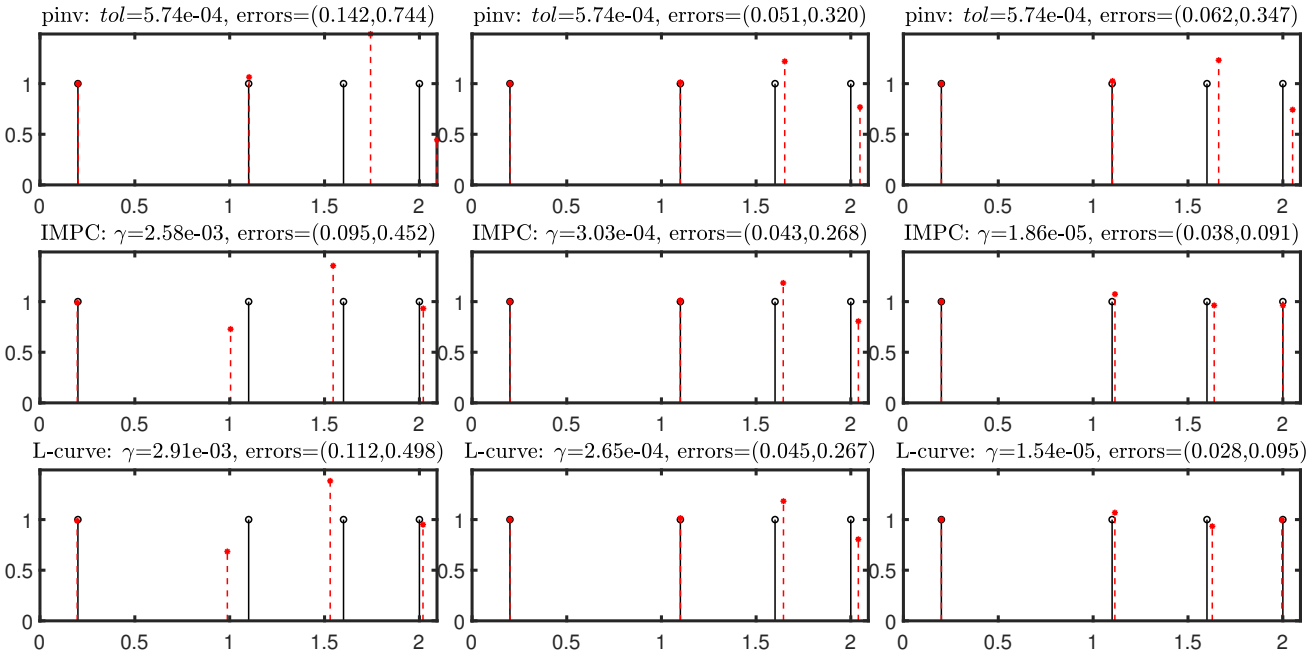

Figure 4. Laplace inversion (columns from left to right: $\sigma = 10^{-3}, 10^{-4}, 10^{-5}$). The exact spikes are in a solid line and the recovered spikes are in a dashed line. The errors measure the 2-norm difference in spike locations and weights, respectively.

Figure 4 shows the reconstructed spike locations and weights in comparison with the exact ones by 3 different methods (denoted by pinv, IMPC, and L-curve) with 3 different noise levels. Again, our Tikhonov regularized eigenmatrix methods (both IMPC and L-curve) demonstrate more accurate recovery, which is expected since the most appropriate choice of a threshold tolerance *tol* requires careful tuning by hand.

4.5. Example 5 (Sparse deconvolution)

In this problem, we have $X = [-1, 1]$, $g(s, x) = \frac{1}{1+4(s-x)^2}$, and true spike locations

$$\boldsymbol{x} = [-0.9; 0; 0.5; 0.9].$$

We generated $n_s = 128$ random sampling points $\{s_j\}$ in $[-5, 5]$, and then build the matrix $G = [g(s_j, a_t)]$ with $n_a = 32$ Chebyshev collocation nodes on $[-1, 1]$. Numerically, we notice that $\widehat{G}$ is not of full column rank with $\text{rank}(\widehat{G}) = 31$ and a large condition number $\text{cond}(\widehat{G}) \approx 10^{14}$. Figure 5 displays the reconstructed spike locations and weights in comparison with the exact ones by 3 different methods (denoted by pinv, IMPC, and L-curve) with 3 different noise levels. Again, our Tikhonov regularized eigenmatrix methods (both IMPC and L-curve) provide more accurate recovery.

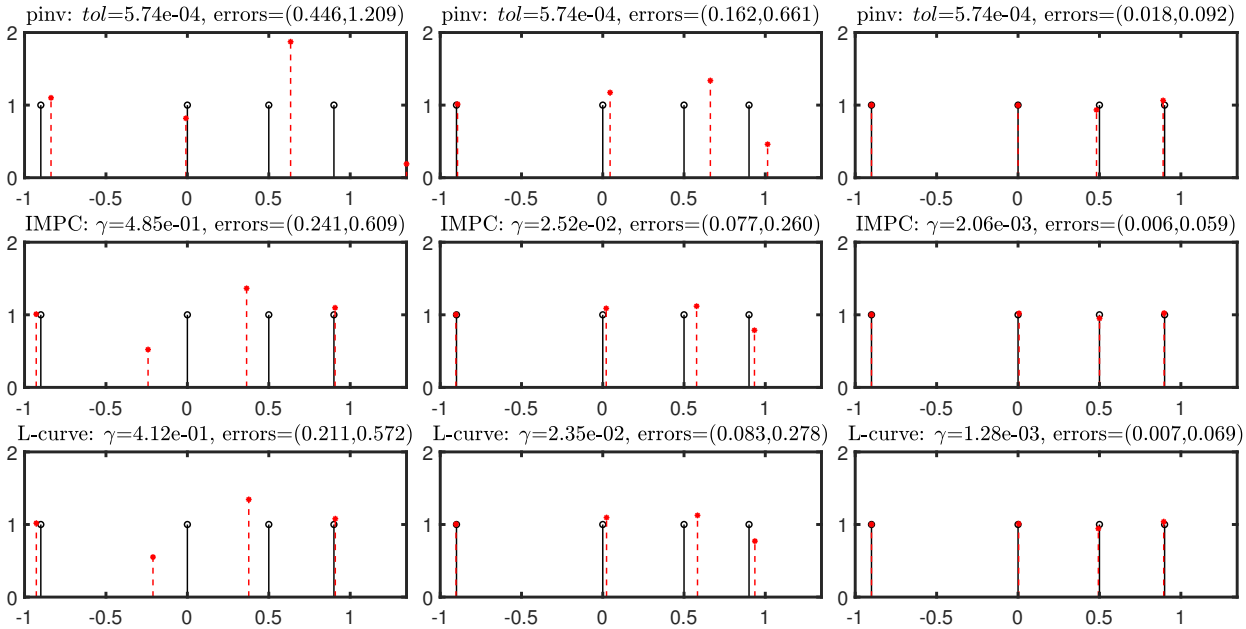

Figure 5. Sparse deconvolution (columns from left to right: $\sigma = 10^{-1}, 10^{-2}, 10^{-3}$). The exact spikes are in a solid line and the recovered spikes are in a dashed line. The errors measure the 2-norm difference in spike locations and weights, respectively.

5. Conclusions

The original eigenmatrix method requires the computation of a pseudo-inverse matrix based on a chosen threshold tolerance, which cannot take into account the noise in data. Our proposed regularized eigenmatrix method addressed this shortcoming by incorporating modern regularization techniques, which provide improved recovery as consistently verified by the numerical examples presented above. The generalization of our approach to multidimensional data recovery problems [38,39] is very straightforward, where the major step of computing $\widehat{G}^{\dagger}\widetilde{\boldsymbol{u}}$ can be treated in the same way without explicitly constructing the pseudo-inverse matrix $\widehat{G}^{\dagger}$. For future work, we will be investigating ways to optimize sampling locations.

Use of AI tools declaration

The authors declare they have not used Artificial Intelligence (AI) tools in the creation of this article.

Acknowledgments

The authors would like to thank the anonymous referees for their valuable comments that have significantly improved the quality and presentation of this paper.

Conflict of interest

The authors declare there is no conflict of interest.

References

1. M. Berljafa, S. Guttel, The RKFIT algorithm for nonlinear rational approximation, *SIAM J. Sci. Comput.*, **39** (2017), A2049–A2071. https://doi.org/10.1137/15M1025426
2. L. Ying, Analytic continuation from limited noisy Matsubara data, *J. Comput. Phys.*, **469** (2022), 111549. https://doi.org/10.1016/j.jcp.2022.111549
3. L. Ying, Pole recovery from noisy data on imaginary axis, *J. Sci. Comput.*, **92** (2022), 107. https://doi.org/10.1007/s10915-022-01963-z
4. D. Potts, M. Tasche, Parameter estimation for exponential sums by approximate Prony method, *Signal Process.*, **90** (2010), 1631–1642. https://doi.org/10.1016/j.sigpro.2009.11.012
5. D. Potts, M. Tasche, Parameter estimation for nonincreasing exponential sums by Prony-like methods, *Linear Algebra Appl.*, **439** (2013), 1024–1039. https://doi.org/10.1016/j.laa.2012.10.036
6. W. T. Weeks, Numerical inversion of Laplace transforms using Laguerre functions, *J. ACM*, **13** (1966), 419–429. https://doi.org/10.1145/321341.321351
7. B. Davies, B. Martin, Numerical inversion of the Laplace transform: a survey and comparison of methods, *J. Comput. Phys.*, **33** (1979), 1–32. https://doi.org/10.1016/0021-9991(79)90025-1
8. T. Peter, G. Plonka, A generalized Prony method for reconstruction of sparse sums of eigenfunctions of linear operators, *Inverse Probl.*, **29** (2013), 025001. https://doi.org/10.1088/0266-5611/29/2/025001
9. A. Cohen, *Numerical Methods for Laplace Transform Inversion*, Springer New York, 2007.
10. S. Becker, J. Bobin, E. J. Candès, NESTA: a fast and accurate first-order method for sparse recovery, *SIAM J. Imag. Sci.*, **4** (2011), 1–39. https://doi.org/10.1137/090756855
11. E. C. Marques, N. Maciel, L. Naviner, H. Cai, J. Yang, A review of sparse recovery algorithms, *IEEE Access*, **7** (2018), 1300–1322. https://doi.org/10.1109/ACCESS.2018.2886471
12. L. Ying, Eigenmatrix for unstructured sparse recovery, *Appl. Comput. Harmon. Anal.*, **71** (2024), 101653. https://doi.org/10.1016/j.acha.2024.101653

13. R. Roy, T. Kailath, ESPRIT-estimation of signal parameters via rotational invariance techniques, *IEEE Trans. Acoust. Speech Signal Process.*, **37** (1989), 984–995. https://doi.org/10.1109/29.32276

14. H. Akaike, Information theory and an extension of the maximum likelihood principle, in *Selected Papers of Hirotugu Akaike*, Springer, (1998), 199–213. https://doi.org/10.1007/978-1-4612-1694-0_15

15. G. Schwarz, Estimating the dimension of a model, *Ann. Stat.*, **6** (1978), 461–464. https://doi.org/10.1214/aos/1176344136

16. R. Schmidt, Multiple emitter location and signal parameter estimation, *IEEE Trans. Antennas Propag.*, **34** (1986), 276–280. https://doi.org/10.1109/TAP.1986.1143830

17. H. W. Engl, M. Hanke, A. Neubauer, *Regularization of Inverse Problems*, Springer Science & Business Media, 1996.

18. P. C. Hansen, Discrete inverse problems: insight and algorithms, *SIAM*, Philadelphia, 2010. https://doi.org/10.1137/1.9780898718836

19. A. Kirsch, *An Introduction to the Mathematical Theory of Inverse Problems*, Springer New York, 2011.

20. M. Benning, M. Burger, Modern regularization methods for inverse problems, *Acta Numer.*, **27** (2018), 1–111. https://doi.org/10.1017/S0962492918000016

21. K. Ito, B. Jin, Inverse problems: Tikhonov theory and algorithms, World Scientific, 2014.

22. H. W. Engl, Discrepancy principles for Tikhonov regularization of ill-posed problems leading to optimal convergence rates, *J. Optim. Theory Appl.*, **52** (1987), 209–215. https://doi.org/10.1007/BF00941281

23. F. S. V. Bazán, J. B. Francisco, An improved fixed-point algorithm for determining a Tikhonov regularization parameter, *Inverse Probl.*, **25** (2009), 045007. https://doi.org/10.1088/0266-5611/25/4/045007

24. P. C. Hansen, Analysis of discrete ill-posed problems by means of the L-curve, *SIAM Rev.*, **34** (1992), 561–580. https://doi.org/10.1137/1034115

25. H. W. Engl, W. Grever, Using the L–curve for determining optimal regularization parameters, *Numer. Math.*, **69** (1994), 25–31. https://doi.org/10.1007/s002110050078

26. P. C. Hansen, J. S. Jørgensen, AIR Tools II: algebraic iterative reconstruction methods, improved implementation, *Numerical Algorithms*, **79** (2018), 107–137. https://doi.org/10.1007/s11075-017-0430-x

27. S. Gazzola, P. C. Hansen, J. G. Nagy, IR tools: a MATLAB package of iterative regularization methods and large-scale test problems, *Numerical Algorithms*, **81** (2019), 773–811. https://doi.org/10.1007/s11075-018-0570-7

28. U. Tautenhahn, On the asymptotical regularization of nonlinear ill-posed problems, *Inverse Probl.*, **10** (1994), 1405–1418. https://doi.org/10.1088/0266-5611/10/6/014

29. Y. Zhang, C. Chen, Stochastic asymptotical regularization for linear inverse problems, *Inverse Probl.*, **39** (2023), 015007. https://doi.org/10.1088/1361-6420/aca70f

30. A. Neubauer, On Nesterov acceleration for Landweber iteration of linear ill-posed problems, *J. Inverse Ill-Posed Probl.*, **25** (2016), 381–390. https://doi.org/10.1515/jiip-2016-0060

31. R. Gong, B. Hofmann, Y. Zhang, A new class of accelerated regularization methods, with application to bioluminescence tomography, *Inverse Probl.*, **36** (2020), 055013. https://doi.org/10.1088/1361-6420/ab730b

32. H. Robbins, S. Monro, A stochastic approximation method, *Ann. Math. Stat.*, **22** (1951), 400–407. https://doi.org/10.1214/aoms/1177729586

33. H. Maurer, K. Holliger, D. E. Boerner, Stochastic regularization: smoothness or similarity? *Geophys. Res. Lett.*, **25** (1998), 2889–2892. https://doi.org/10.1029/98GL02183

34. B. Jin, X. Lu, On the regularizing property of stochastic gradient descent, *Inverse Probl.*, **35** (2019), 015004. https://doi.org/10.1088/1361-6420/aaea2a

35. H. G. Moura, E. C. Junior, A. Lenzi, V. C. Rispoli, On a stochastic regularization technique for ill-conditioned linear systems, *Open Eng.*, **9** (2019), 52–60. https://doi.org/10.1515/eng-2019-0008

36. B. Jin, Z. Zhou, J. Zou, On the convergence of stochastic gradient descent for nonlinear ill-posed problems, *SIAM J. Optim.*, **30** (2020), 1421–1450. https://doi.org/10.1137/19M1271798

37. H. Choi, A. Thite, D. Thompson, A threshold for the use of Tikhonov regularization in inverse force determination, *Appl. Acoust.*, **67** (2006), 700–719. https://doi.org/10.1016/j.apacoust.2005.11.003

38. L. Ying, Multidimensional unstructured sparse recovery via eigenmatrix, preprint, arXiv:2402.17215.

39. F. Andersson, M. Carlsson, ESPRIT for multidimensional general grids, *SIAM J. Matrix Anal. Appl.*, **39** (2018), 1470–1488. https://doi.org/10.1137/17M1137267

AIMS Press